

# Role of spin-orbit coupling and evolution of the electronic structure of $\text{WTe}_2$ under an external magnetic field

D. Rhodes,<sup>1</sup> S. Das,<sup>2</sup> Q. R. Zhang,<sup>1</sup> B. Zeng,<sup>1</sup> N. R. Pradhan,<sup>1</sup> N. Kikugawa,<sup>3,1</sup> E. Manousakis,<sup>2,4</sup> and L. Balicas<sup>1,\*</sup>

<sup>1</sup>*National High Magnetic Field Laboratory, Florida State University, Tallahassee-FL 32310, USA*

<sup>2</sup>*Department of Physics and National High Magnetic Field Laboratory,  
Florida State University, Tallahassee-FL 32310, USA*

<sup>3</sup>*National Institute for Materials Science, Tsukuba, Ibaraki 305-0047, Japan*

<sup>4</sup>*Department of Physics, University of Athens, Panepistimioupolis, Zografos, 157 84 Athens, Greece*

(Dated: December 3, 2024)

Here, we present a detailed study on the temperature and angular dependence of the Shubnikov-de-Haas (SdH) effect in the semi-metal  $\text{WTe}_2$ . This compound was recently shown to display a very large non-saturating magnetoresistance which was attributed to nearly perfectly compensated densities of electrons and holes. We observe four fundamental SdH frequencies and attribute them to spin-orbit split, electron- and hole-like, Fermi surface (FS) cross-sectional areas. Their angular dependence is mildly consistent with ellipsoidal FSs with volumes implying an excess of  $\sim 7\%$  in the density of electrons with respect to that of the holes. Nevertheless, we show that density functional theory (DFT) calculations can reasonably describe the experimentally determined electron FSs but fail to accurately describe the hole FSs. When their cross-sectional areas are adjusted to reflect the experimental data, the resulting volumes of the electron/hole FSs obtained from the DFT would imply a strong imbalance between the densities of electrons and holes. We observe a severe field-induced renormalization of the effective masses suggesting that the electronic structure of  $\text{WTe}_2$  is particularly sensitive to the Zeeman-effect. By combining the results of our DFT calculations with our analysis of the experimental results we conclude that  $\text{WTe}_2$  is unlikely to remain compensated under an external field.

## I. INTRODUCTION

Transition metal dichalcogenides  $\text{TMX}_2$  (where  $\text{TM}$  stands for a transition metal, and  $\text{X}$  for a chalcogen) became the subject of intense research activity since, as graphene, they can be exfoliated into a single monolayer which[1], in the case of semiconducting compounds, present remarkable optoelectronic properties[2]. These compounds present a wide range of electronic states[1], from wide gap semiconductors such as trigonal  $1T\text{-HfS}_2$ [3], to semiconductors presenting band gaps comparable to Si such as  $\alpha\text{-MoTe}_2$ [4], to Mott systems such as  $1T\text{-TaS}_2$ [5], to charge-density wave(s) coexisting with superconductivity as in  $2H\text{-NbSe}_2$ [6], to semi-metals such as  $\beta\text{-MoTe}_2$  or  $\text{WTe}_2$ [7].

$\text{WTe}_2$ , which crystallizes in a distorted, orthorhombic variant of the  $\text{CdI}_2$  structure with octahedral coordination around W, was recently reported to display an extremely pronounced and non-saturating magnetoresistance which[7], following arguments discussed by Pippard[8], was attributed to a nearly perfect compensation between the density of electrons and holes. Evidence for electron/hole compensation was recently provided by angle-resolved photoemission (ARPES) experiments which claim to observe electron- and hole-like Fermi surface pockets of almost the same size[9]. These results contrast markedly with a subsequent ARPES study[10] which claim to observe up to 9 FS sheets, including a hole-pocket at the Brillouin zone center or the  $\Gamma$ -point,

and two hole-pockets and two electron-pockets on each side of  $\Gamma$  and along the  $\Gamma$ -X direction. The same study finds evidence for spin-orbit split bands and for an opposite texture between the spin and the angular orbital momentum around the  $\Gamma$ -point which should suppress carrier backscattering[10]. The application of a magnetic field would not only alter the spin texture, it would also displace, through the Zeeman effect, the spin-split bands relative to the Fermi level, opening backscattering channels and hence increasing the resistivity. Similar arguments were invoked to explain the pronounced magnetoresistivity observed in  $\text{Cd}_3\text{As}_2$ [11].

Electrical transport studies focused on the Shubnikov-de Haas-effect, or the quantum oscillatory phenomena superimposed onto the magnetoresistive behavior which results from the Landau quantization of the electronic orbits, yield results that contrast markedly with both ARPES studies[12, 13]. The first study reports the observation of just 3 Fermi surface pockets in marked contrast also with band structure calculations which always predict an even number of FS pockets for bulk  $\text{WTe}_2$ [9, 13, 14]. The second, more in line with the calculations, observe 4 Fermi surface pockets, or two sets of concentric electron- and hole-like FSs[13]. The angular dependence of the observed frequencies, or of the FS cross-sectional areas obtained from the Onsager relation, suggests ellipsoidal pockets with volumes yielding an excess of 4 % in the density of holes when compared that of the electrons. This imbalance would be comparable to that of elemental Bi which in contrast to  $\text{WTe}_2$  displays a saturating magnetoresistance[15].

Here, we present angle- and temperature-dependent

\* balicas@magnet.fsu.edu

magnetoresistivity measurements in fields up to  $H = 35$  T on  $\text{WTe}_2$  single-crystals, in an attempt to elucidate the number of Fermi surface sheets. In parallel, we performed density-functional theory (DFT) calculations incorporating the spin-orbit effect, and by adjusting the position of the chemical potential we attempted to precisely describe the geometry of the measured Fermi surfaces. In agreement with a previous report[13] we observe four fundamental frequencies, or Fermi surface cross-sectional areas, which we ascribe to spin-orbit split electron- and hole-pockets. Although, and as argued in Ref. 13, their angular dependence can be described in terms of ellipsoidal FSs, we find that the electron FSs can be relatively well-described by the DFT calculations, while such calculations fail to accurately and fully describe the angular dependence of the hole-pockets. In neither FS description the concomitant densities of holes and electrons are perfectly compensated. Finally, we provide evidence indicating that for fields aligned along the  $c$ - and the  $b$ -axis the effective masses are severely renormalized by the field, i.e. become considerably heavier. The DFT calculations indicate that the evolution of the electronic structure at the Fermi level due to the Zeeman-effect, is likely to play a determinant role in the non-saturating magnetoresistance displayed by  $\text{WTe}_2$ .

## II. EXPERIMENTAL

$\text{WTe}_2$  was grown via a chemical vapor transport technique using chlorine as the transport agent: W (99.999 %) and Te (99.9999 %) were heated up to a peak temperature of 750 °C at a rate of 100 °C/h, and subsequently cooled down to room temperature at a rate of 10 °C/h. The obtained powder was ground with a mortar and pestle and heated again following the the same temperature profile. The remaining product was subsequently combined with  $\text{TeCl}_4$  (99.999 %, 1.5 mg/cm<sup>3</sup>) and heated up to a peak temperature of 750 °C at a rate of 100 °C/h under a temperature gradient of  $\approx 50$  °C. The crystals used for this study displayed resistivity ratios in excess of  $10^2$ . Subsequent crystals grown via the Te flux method, yielded much higher RRRs ( $\sim 700$ ) and show similar behavior (see supplementary information).

The synthesis procedure yielded platelet like single crystals, several millimeters in length and typically a millimeter wide, making the  $a$ -,  $b$ -, and the  $c$ -axis easily distinguishable. The stoichiometric composition was determined by energy dispersive  $X$ -ray spectroscopy and single-crystal  $X$ -ray refinement. A conventional four terminal configuration was used for the resistivity measurements which were performed under high magnetic-fields either by using a 35 T resistive magnet or a Physical Property Measurement System (PPMS).

Figures 1 (a), (b), and (c) show the resistivity  $\rho$  of a  $\text{WTe}_2$  single-crystal as a function of the magnetic field applied along the  $a$ ,  $b$ , and  $c$ -axis respectively, for several temperatures and with the electrical cur-

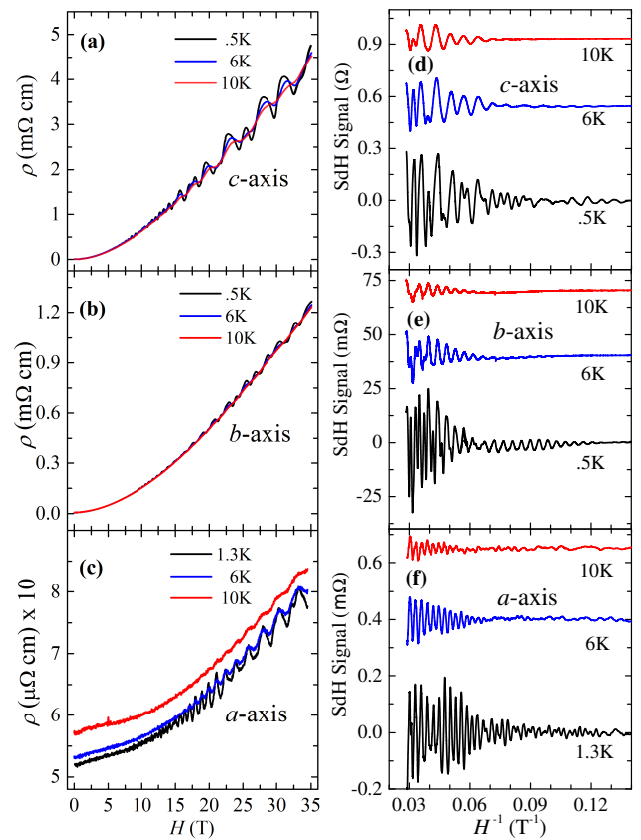


FIG. 1. (a) Resistivity  $\rho$  as a function of the magnetic field  $H$  applied along the  $c$ -axis, for a  $\text{WTe}_2$  single-crystal and for three representative values of the temperature  $T$ , i.e. 0.5 K (black line), 6 K (blue) and 10 K (red), respectively. Here, the current is applied along the  $a$ -axis, hence perpendicularly to  $H$ . (b) Same as in (a) but for fields along the  $b$ -axis of the crystal. (c) Same as in (a) but for currents parallel to  $H$  which is applied along the  $a$ -axis. (d) Shubnikov-de-Haas signal superimposed onto the curves in (a) after subtraction of a polynomial background. (e) Same as in (d) but from the curves in (b). (f) Same as in (d) but from the curves in (c).

rent applied along the  $a$ -axis. In agreement with previous reports[7, 13], fields along the  $c$ -axis yields the largest magnetoresistivity, although in our crystals the anisotropy in magnetoresistivity between fields along the  $c$ - and the  $b$ -axis is just a factor of 4 and not beyond one order of magnitude[13]. The smallest change in resistivity is observed for fields applied along the  $a$ -axis since in this configuration the Lorentz force is expected to vanish. For all three sets of data the oscillatory component superimposed into the smoothly increasing background corresponds to the Shubnikov-de-Haas effect. Figures 1 (d), (e), (f), display the oscillatory component superimposed onto  $\rho(H, T)$  as a function of the inverse field  $H^{-1}$ , for fields oriented along all three crystallographic axes and for several temperatures (from the curves in (a), (b) and (c), respectively). To obtain the oscillatory component, the smoothly varying background was fit to a polynomial

which was subsequently subtracted from the raw data.

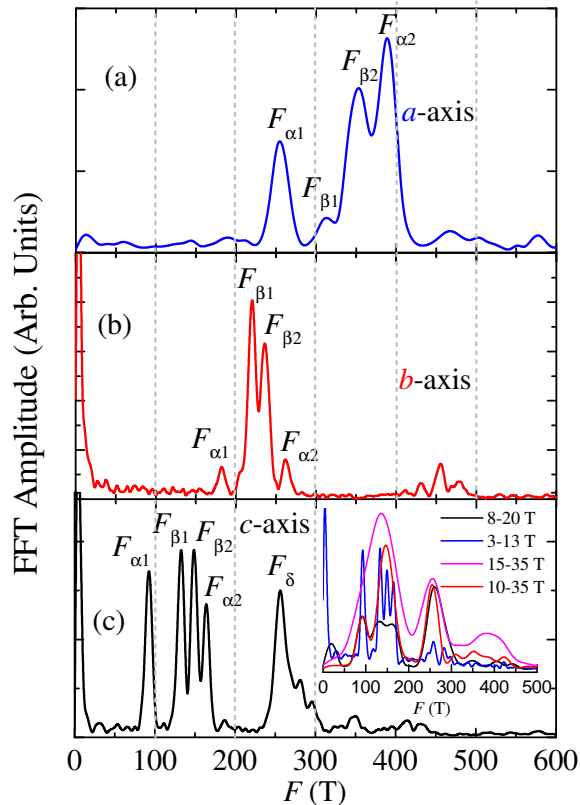


FIG. 2. (a) Fast Fourier transform of the SdH signal superimposed onto  $\rho(H)$  for fields along the  $a$ -axis and for  $T = 1.3$  K. Here, the oscillatory signal was extracted from a field interval ranging from 3 to 35 T. As is discussed in the main text, the indexing of the four peaks observed in the FFT spectrum is based upon band structure calculations, where  $F_\alpha$  and  $F_\beta$  denotes hole- and electron-pockets respectively, and the indexes 1 and 2 differentiate spin-orbit split Fermi surface pockets. (b) Same as in (a) but for fields along the  $b$ -axis and for  $T = 0.5$  K. (c) Same as in (a) but for fields along the  $c$ -axis and for  $T = 0.5$  K. Inset: FFT spectra extracted for different field intervals. Notice the loss of frequency resolution when the FFT is extracted either from traces acquired under high fields or from a limited field range. To allow the visual comparison between the different FFT spectra the blue and black traces were multiplied by a factor 75 and 3.5, respectively. Notice how within the interval  $\Delta H = 8 - 20$  T the peak corresponding to the magnetic breakdown orbit  $F_\delta$  becomes more pronounced than the fundamental peaks.

Figures 2 (a), (b), and (c) show the fast Fourier transform (FFT) of the SdH oscillatory signal displayed in Figs. 1 (d), (e), and (f), respectively. As seen, for fields along all three crystallographic axes four fundamental frequencies are clearly observed. This is in agreement with the observations of Ref. 13 but contrasts markedly with both ARPES studies 9 and 10. For fields along the  $c$ -axis one observes peak frequencies at  $F_{\alpha 1} = 90$  T,  $F_{\beta 1} = 130$  T,  $F_{\beta 2} = 145$  T, and  $F_{\alpha 2} = 160$  T, respec-

tively. As we discuss below, and based on DFT calculations, the  $\alpha$  and the  $\beta$  frequencies are identified with spin-orbit split hole- and electron-pockets, respectively. The indexes 1 and 2 distinguish the smaller from the larger spin-orbit split Fermi surfaces. We see a gradual increase in the frequencies as the crystal is rotated from  $c$ - towards the  $b$ -axis or the  $a$ -axis. For fields along the  $b$ -axis the peaks are shifted towards  $F_{\alpha 1} = 180$  T,  $F_{\beta 1} = 220$  T,  $F_{\beta 2} = 236$  T, and  $F_{\alpha 2} = 262$  T, respectively. For fields along the  $a$ -axis the peaks are observed at  $F_{\alpha 1} = 250$  T,  $F_{\beta 1} = 300$  T,  $F_{\beta 2} = 357$  T, and  $F_{\alpha 2} = 390$  T, respectively.

For fields along the  $c$ -axis one observes also a pronounced fifth peak,  $F_\delta \simeq 250$  T, which clearly corresponds to  $F_{\alpha 1} + F_{\alpha 2}$ , previously attributed to magnetic breakdown or to the magnetic field-induced carrier tunneling between both orbits[13]. The fact that the amplitude of the peak associated with  $F_\delta$  is more pronounced than peaks associated with the fundamental orbits, such as  $F_{\alpha 2}$ , contradicts this scenario. Unless both concentric FS sheets were in close proximity at the point of nearly touching. In fact, as seen in the inset of Fig. 2 (c), which displays the FFT spectra acquired under distinct field intervals, this orbit becomes progressively more pronounced at higher fields, which is consistent with magnetic breakdown. However, as illustrated by the FFT spectrum extracted from the field interval ranging from 8 to 20 T, the amplitude of  $F_\delta$  can, in some field intervals, become more pronounced than the amplitude of all other fundamental peaks. This suggests that the Zeeman-effect is altering the geometry of the  $\alpha$ -pockets, hence decreasing their (spin-orbit induced) splitting in some region(s) of  $k$ -space. Our DFT analysis, discussed below, is indeed consistent with this possibility. This would imply that the electronic structure at the Fermi level evolves with field due to the Zeeman-effect. We considered this hypothesis and evaluated the possibility of studying in detail the evolution of the SdH frequencies, and of the concomitant effective masses, as a function of the field. But as illustrated by the inset of Fig. 2 (c), the resolution among peaks in the FFT spectra, or the peak sharpness, decreases considerably when the very low field interval is excluded from the oscillatory signal, thus preventing such a detailed analysis.

Figures 3 (a), (b), and (c) display the amplitude of each peak observed in the FFT spectra as a function of the temperature  $T$ , for fields along the  $a$ -,  $b$ -, and the  $c$ -axis, respectively. Solid lines are fits to the Lifshitz-Kosevich formula  $A/\sinh X$  (where  $X = 2\pi^2 k_B T/\hbar\omega_c = 14.69\mu T/\overline{H}$ , with  $\mu$  being the effective mass  $\mu$  and  $\overline{H}$  the average field value), from which we extract the effective masses. As seen, the fits are excellent yielding precise values for  $\mu$ . More importantly, according to the fits in Fig. 3 (d), the effective mass of  $F_\delta$ , or  $\mu_\delta$ , is found to evolve as a function of the field: i.e.  $\mu_\delta = (0.73 \pm 0.05)m_0$  for  $H$  ranging from 3 to 13 T,  $\mu_\delta = (0.9 \pm 0.07)m_0$  for fields between 8 and 20 T,  $\mu_\delta = (0.97 \pm 0.02)m_0$  for fields ranging from 15 to 35 T. In Table I below summarizes

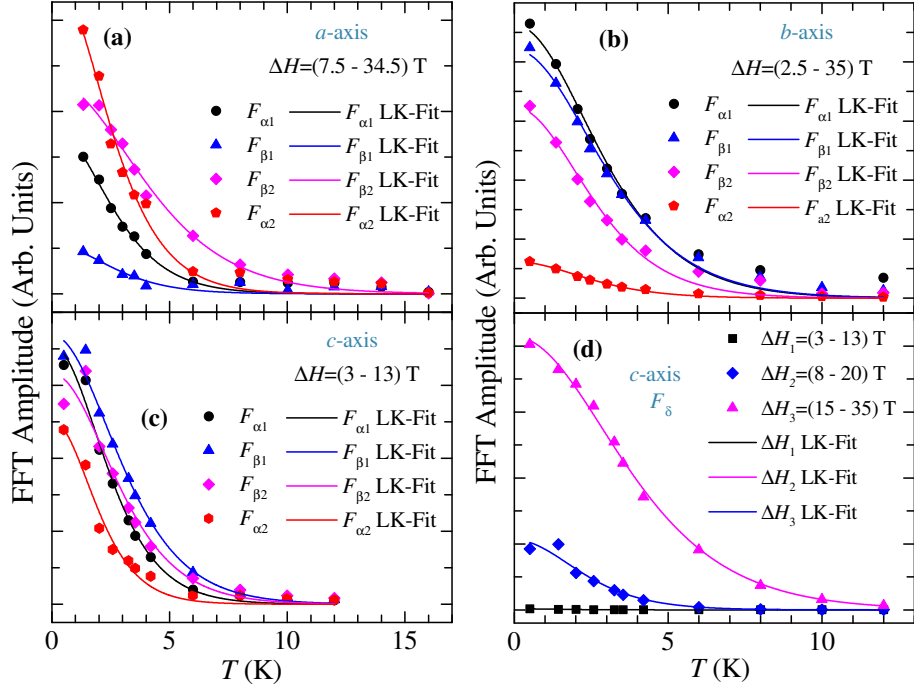


FIG. 3. (a) Magnitude of the FFT peaks extracted from the oscillatory component superimposed into the magnetoresistivity measured for fields applied along the  $a$ -axis and as a function of the temperature  $T$ . Solid lines are linear fits to the Lifshitz-Kosevich formalism from which we extract the effective masses  $\mu$ . (b) Same as in (a) but for fields along the  $b$ -axis. (c) Same as in (a) but for fields along the  $c$ -axis. (d) Magnitude of FFT peak observed at  $F_{\delta}$  which corresponds to a magnetic breakdown orbit.

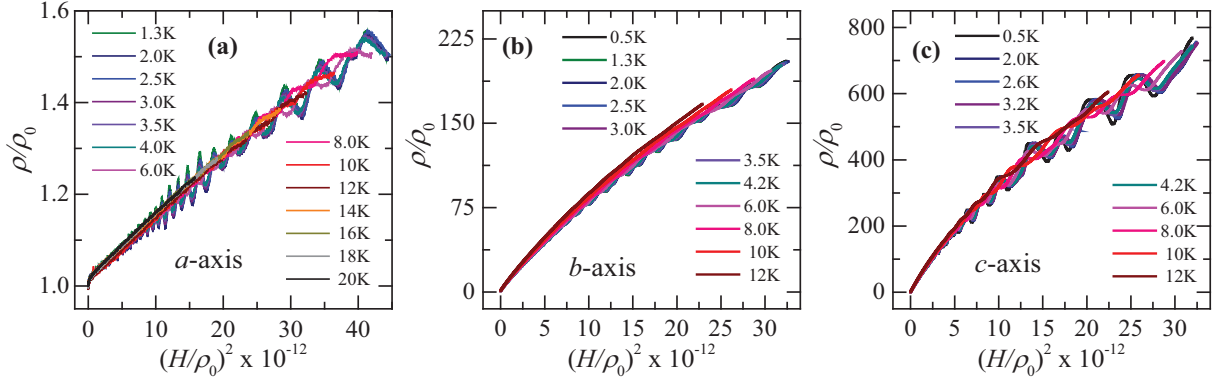


FIG. 4. (a) Kohler plot of the resistivity  $\rho$ , normalized by its zero field value  $\rho_0$ , as a function of  $(H/\rho_0)^2$  for fields applied along the  $a$ -axis. (b) Same as in (a) but for fields along the  $b$ -axis. (c) Same as in (a) but for fields along the  $c$ -axis.

the experimental information extracted from this study, including effective masses for  $H \parallel c$ - and to the  $b$ -axis, in each case extracted from two intervals in field, i.e. a low field region and the whole field window up to 35 T. As seen, the effective masses extracted from the whole field range are approximately a factor of 2 heavier than those extracted from the low field region, clearly indicating a severe effective mass renormalization induced by the application of a magnetic field. In the same table we include the results of an attempt to match the experi-

mentally determined FSs with those determined from the DFT calculations by independently adjusting the position of the electron- and hole-bands relative to the Fermi level.

Finally we show in Fig. 4 Kohler plots of the resistivity  $\rho$  normalized by its zero field value  $\rho_0$  as a function of the square of the field  $H^2$  normalized by  $\rho_0$  and for fields along all three crystallographic orientations. Recently, it was claimed[23] that  $\text{WTe}_2$  would *not* obey the Kohler rule[8], leading to an anomalous linear magnetoresistance

for currents parallel to the field. However, as seen in Fig. 4, our data clearly follows Kohler scaling with very mild deviations for fields along the  $b$ -axis, and only for the curves taken at higher temperatures. At lower fields, and for fields along the  $a$ -axis, indeed  $\rho(H) \sim H$ . Since for this current/field configuration the Lorentz force is nearly zero, which leads to no orbital magnetoresistivity, a very careful experimental effort, such as very precise field-alignment and homogeneous current distribution will be required to characterize this effect. The fact that  $\text{WTe}_2$  nearly obeys Kohler rule for all three crystallographic orientations implies that its orbital magnetoresistivity is dominated by scattering by phonons and impurities.

### III. DFT CALCULATIONS AND THE EVOLUTION OF THE FERMI SURFACES

One of the main goals of this study is to compare the geometry of the experimentally detected FSs with those resulting from *ab-initio* calculations such as the ones included in Refs. 7, 9, 13, and 14. Notice that the initial calculations [7, 9, 14] ignored spin-orbit coupling implying the existence of one hole- and one electron-like pocket. This would be at odds with the results reported by Ref. 13. Electronic structure calculations were performed by using the Vienna *ab-initio* simulation package [16–19] (VASP) within the generalized gradient approximation (GGA). We have included the contribution of spin-orbit coupling in our calculations. The Perdew-Burke-Ernzerhof (PBE) exchange correlation functional [20] and the projected augmented wave (PAW) methodology [21] was used to describe the core electrons. The  $5d$  and  $6s$  electrons for W and the  $5s$  and  $5p$  electrons for Te were treated as valence electrons in all our calculations. The energy cut off for the plane-wave basis was chosen to be 600 meV. A total of 96 bands and a  $k$ -point mesh of  $8 \times 8 \times 8$  were used for the self-consistent ground state calculations. A total of 100  $k$ -points were chosen between each pair of special  $k$ -points in the Brillouin-zone for the band-structure calculations.

In order to obtain an accurate and detailed representation of the Fermi surface we have used a  $80 \times 80 \times 80$   $k$ -point mesh. The areas of the observed and calculated FS orbits are related to the SdH frequencies by the Onsager relation,

$$F_{\vec{k}} = \frac{\phi_0}{2\pi^2} A_{\vec{k}} \quad (1)$$

where  $\phi_0 = 2.07 \times 10^{-15} \text{ Tm}^2$  is the quantum of flux and  $A_{\vec{k}}$  is the area of the electron orbit perpendicular to the field. The effective masses of the electron- and the hole-pockets at these extremal orbits are determined by using the relation:

$$m_k^*(\epsilon) = \frac{\hbar^2}{2\pi} \frac{\partial A_k(\epsilon)}{\partial \epsilon}. \quad (2)$$

We have calculated the areas of the orbits by considering cuts of the Fermi surface with planes intersecting the Fermi surface perpendicularly to the  $a$ -,  $b$ - and the  $c$ -axis at various different angles. In an attempt to match the experimentally observed FSs with the calculated ones, we chose to adjust our calculations to the experimental cross-sections obtained for fields along the  $c$ -axis. For this, the energy of the electron pockets were down shifted with respect to the Fermi level by an amount of 25 meV, while the hole pockets were displaced upwards by 20 meV. The Fermi surfaces were generated using the eigenvalues obtained from VASP and were visualized using the XCrysden software [22]. As seen in Fig. III, the resulting Fermi surface is composed of two sets of spin-orbit split pockets at either side of the  $\Gamma$ -point and along the  $\Gamma$ -X direction, with the electron-like pockets being depicted in blue or clear blue color, and the hole-like in red or in clear and nearly transparent red.

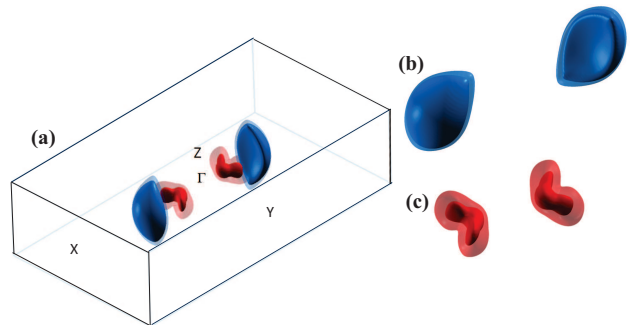


FIG. 5. (a) Fermi surface of  $\text{WTe}_2$ . The spin-orbit split electron pockets are shown in blue, and in transparent light blue color, respectively. The hole pockets are shown in red and in pink color. The position of the energy of the electron and hole pockets was independently adjusted to obtain a good agreement with the experimentally observed Shubnikov de Haas frequencies for magnetic fields along the  $c$ -axis. In order to obtain high resolution, the size of the  $k$ -point mesh used was  $80 \times 80 \times 80$ . This is required to obtain, as accurately as possible, the angle dependence of the frequencies for both electron and hole orbits. The reason for 2 electron- and 2 hole-like pockets, as opposed to just two doubly degenerate ones, is the spin-orbit coupling. Therefore, the spin-orbit coupling is particularly large (relative to the energy dispersion near the Fermi level) for the hole pockets. (b) The electron pockets are shown in a higher resolution, larger image. (c) Same as in (b) but for the hole-pockets.

In Table I below, we summarize the experimental results as well as those resulting from the DFT calculations. In particular, we present a comparison between the experimental effective masses  $\mu$ , extracted from the fits in Fig. 3, and the band masses  $\mu^b$  resulting from the DFT calculations. Here, the important observation is not only the marked contrast between the band masses and the experimental effective-masses with the band masses being systematically heavier (in particular for the  $\alpha$ -orbits), but also their field dependence. As seen in Table I, the

effective masses are strongly field dependent, increasing by nearly a factor of 2 when they are extracted from the whole field range as compared with the masses extracted from the low field region. This is a very clear indication for the role of the Zeeman-effect in altering the electronic structure at the Fermi level and in leading to a concomitant increase in the density of states at the Fermi level  $\rho(E_F)$ . For samples that start to display quantum oscillatory behavior under fields  $H < 3$  T it is remarkable,

as seen in the inset of Fig. 2 (c), that one cannot resolve all four peaks in the FFT spectrum when it is taken over a broad range in  $H$ , such as  $H = 10 \rightarrow 35$  T. However, as illustrated in the Supplemental Material [24] through simple simulations of the experimental data, this just reflects the much lower number of oscillations within this inverse field range when compared to the number of oscillations observed in fields ranging from  $< 3$  T up to 9 T.

	$\mu_a^b$	$\mu_a$ (7.5 $\rightarrow$ 35) T	$\mu_b^b$	$\mu_b$ (3 $\rightarrow$ 13) T	$\mu_b$ (4 $\rightarrow$ 35) T	$\mu_c^b$	$\mu_c$ (3 $\rightarrow$ 9) T	$\mu_c$ (3 $\rightarrow$ 35) T	$n_{\text{ellip.}}$	$n_{\text{DFT}}$
$F_{\alpha 1}$	1.37	(1.17 $\pm$ 0.06)	0.84	(0.44 $\pm$ 0.11)	(0.97 $\pm$ 0.04)	0.72	(0.42 $\pm$ 0.01)	(0.79 $\pm$ 0.04)	0.57	0.78
$F_{\alpha 2}$	1.32	(1.20 $\pm$ 0.07)	1.02	(0.44 $\pm$ 0.05)	(1.13 $\pm$ 0.05)	1.1	(0.47 $\pm$ 0.02)	(0.95 $\pm$ 0.05)	1.15	2.31
$F_{\beta 1}$	1.02	(0.64 $\pm$ 0.14)	0.56	(0.49 $\pm$ 0.01)	(0.84 $\pm$ 0.03)	0.43	(0.33 $\pm$ 0.01)	(0.62 $\pm$ 0.03)	0.84	3.9
$F_{\beta 2}$	0.97	(0.75 $\pm$ 0.04)	0.57	(0.58 $\pm$ 0.03)	(0.92 $\pm$ 0.04)	0.51	(0.36 $\pm$ 0.01)	(0.64 $\pm$ 0.04)	1	5.14

TABLE I. Comparison between the experimental results and the results of the DFT-calculations.  $\mu_{a,b,c}^b$  are the band masses from the DFT calculations for orbits perpendicular to fields applied along all three crystallographic axes (in units of free electron mass  $m_0$ ),  $\mu_{a,b,c}$  are the experimental effective-masses,  $n_{\text{ellip.}}$  are the carrier densities as estimated from a simple ellipsoidal approximation of the Fermi surfaces, and  $n_{\text{DFT}}$  are the carrier densities resulting from the DFT calculations. The  $ns$  are expressed in units of  $10^{19} \text{ cm}^{-3}$ .

Table I also shows the density of carriers  $n_{\text{ellip.}}$  that one would extract from our experiments by assuming ellipsoidal FS pockets[13]. Here, we approximated the FS cross-sectional areas to circles and used the above Onsager relation to extract the respective Fermi vectors  $k_F^{a,b,c}$  along all three crystallographic orientations. The volume of the FS pocket is estimated through the expression for the volume of an ellipsoid, i.e.  $V_{\text{FS}} = 4\pi k_F^a k_F^b k_F^c / 3$ . To extract  $n_{\text{ellip.}}$  one normalizes by the volume of the Brillouin zone. This simple estimation yields a 7% larger density of electrons with respect to that of the holes. This would imply that *under an external field* WTe<sub>2</sub> is *not* perfectly compensated[7, 9]. The FSs calculated by DFT, and subsequently adjusted to match the experimental results, lead to a much worse situation, with the density of electrons becoming  $\sim 3$  times larger than the density of holes.

In Fig. 6 the geometry of the FS is compared to the geometry of the DFT calculated FSs. Figure 6 shows the position of the four fundamental peaks found if the FFT spectra of the SdH signal as a function of the angle relative to the crystallographic  $c$ -axis. Here,  $0^\circ$  corresponds to the  $c$ -axis and  $\pm 90^\circ$  corresponds to either the  $a$ - or the  $b$ -axis. Solid lines depict the angular dependence of the frequencies resulting from our DFT calculations for both the hole- and the electron-pockets including spin-orbit coupling. These curves were obtained by a polynomial fit of their calculated values at discrete angles. Our calculations yield a relatively good agreement with the experimentally obtained frequencies for fields along the

$c$ -axis, and also with the angular dependence of the frequencies corresponding to the electron-pockets. Nevertheless, it shows a very poor agreement with the angular dependence of the frequencies associated with the hole-pockets. Their angular dependence imply very similar geometry for the electron- and the hole-pockets. The orange dashed line is an attempt to fit the observed angular dependence to an ellipsoidal FS. As seen, and as already pointed out by Ref. 13, the experimental data cannot be perfectly described in terms of ellipsoidal pockets. It is however quite remarkable that the DFT calculations also fail to describe the electronic structure of this weakly correlated compound.

In Fig. 7 we illustrate the effect on the geometry of the FSs, of displacements in the position of the Fermi-level by 10 and 20 meV both above and below its original position. These displacements are intended to mimic the role played by the Zeeman-effect on the geometry of the spin-orbit split FSs. Notice that the hole-pockets change significantly by displacing the Fermi level by a small amount in energy, i.e. of the order of just 10 meV, which would correspond to a Zeeman splitting of the order of 50 T. The change is more dramatic when the Fermi level is shifted downward. This exercise implies that the Zeeman-effect would induce pronounced changes in the geometry of the FSs breaking the balance between opposite charge carriers (notice the volume transfer from the hole- to the electron-pockets). Notice also how the hole-pockets extracted from the DFT calculations, which present a boomerang like cross-section, nearly touch at

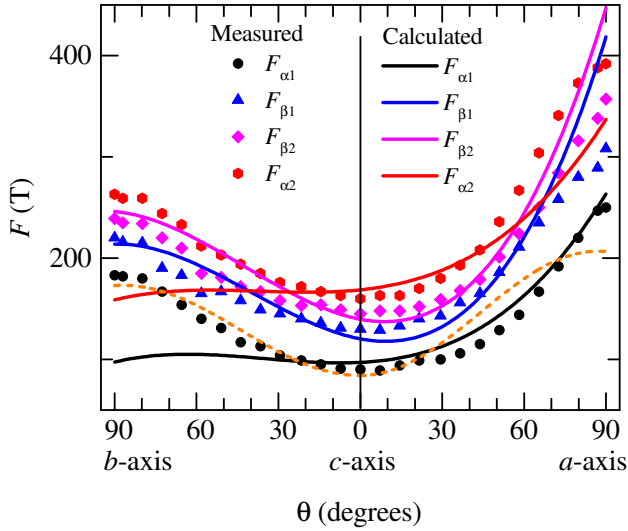


FIG. 6. Position of the main four peaks detected in fast Fourier spectra as a function of the orientation of the field relative to the crystallographic axes. In order to compare experimental results with the theoretical calculations solid lines depict the calculated angular dependence of the frequencies for both electron and hole pockets. Notice the good agreement for the electron- but the poor agreement with the hole-pockets. Orange lines corresponds to a fit assuming an ellipsoidal shape for the smallest Fermi surface which corresponds to the lowest frequency hole pocket.

its vertex when the Fermi level is displaced. This would favor the magnetic breakdown between both orbits as experimentally seen.

#### IV. SUMMARY

In summary, by analyzing the angular dependence of the Shubnikov-de-Haas effect in single-crystals, we detect four Fermi surface cross-sectional areas in the semi-metal  $\text{WTe}_2$  which, based on density functional theory calculations correspond to spin-orbit split electron- and hole-pockets. The angular dependence of the experimental cross-sectional areas associated with the electron pockets is relatively well described by the DFT calculations, indicating that they do not correspond to ellipsoidal pockets. However, *ab-initio* calculations fail to correctly describe the geometry of the hole-pockets whose cross-sectional areas suggest a geometry similar to that of the electron Fermi-surfaces.

More importantly, the experimentally determined effective masses are severely renormalized by the magnetic field, increasing considerably as the field increases. This indicates a severe increase in the density of states at the Fermi level due to a Zeeman-effect induced modification of the electronic structure at the Fermi level. In  $\text{WTe}_2$ , the concomitance between the extremely pronounced magnetoresistivity and the severe renormaliza-

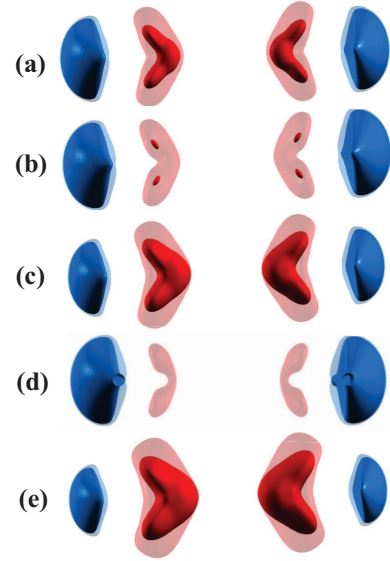


FIG. 7. Evolution of the Fermi surface by shifting the Fermi level by 10 and 20 meV above and below the original Fermi level, respectively. (a) The electron (shown in blue and transparent light blue color) and hole pockets (shown in red and in transparent pink color) for the actual position of the Fermi level. Here, the position of the Fermi level was adjusted to obtain a good agreement with the experimental Shubnikov de Haas frequencies for magnetic fields along the  $c$ -axis. (b) The position of the Fermi level is shifted upward by 10 meV. (c) The position of the Fermi level is shifted downward by 10 meV. (d) The position of the Fermi level is shifted upward by 20 meV. (e) The position of the Fermi level is shifted downward by 20 meV.

tion of the effective mass/density of states at the Fermi level, indicates a Fermi surface that is highly responsive to a magnetic field. This is consistent with our DFT calculations which predict a strong evolution of the Fermi surface as the magnetic field is swept. Even if  $\text{WTe}_2$  was a nearly perfectly compensated semi-metal at zero field[7, 9], our results would imply that it is quite unlikely to remain compensated under the application of an external magnetic field. This spoils the argument that the origin of the observed unsaturated magnetoresistance lies in the perfectly compensated semi-metallic nature of  $\text{WTe}_2$ . In Bi, a nearly compensated semi-metal, a similar effect is believed to lead to its saturating magnetoresistance[13, 15]. Hence, our results imply that an alternative explanation would be required for its “titanic” magnetoresistance, such as the field-induced opening of backscattering channels suggested in Ref. 10.

In a 3D Landau-Fermi liquid, the quasiparticle lifetime is inversely proportional to the quasiparticle energy difference from the Fermi energy[25]. If, upon application of a strong magnetic field the Fermi surface was significantly altered, one should expect a strong influence on the quasiparticle scattering rates and lifetimes, contributing in a non-trivial manner to the enormous magnetoresistance

observed in  $WTe_2$ .

## V. ACKNOWLEDGEMENTS

The NHMFL is supported by NSF through NSF-DMR-1157490 and the State of Florida. LB is supported by

DOE-BES through award DE-SC0002613 and by Army Research Office through the MURI grant W911NF-11-10362.

- 
- [1] M. Chhowalla, H. S. Shin, G. Eda, L. J. Li, K. P. Loh, H. Zhang, *The chemistry of two-dimensional layered transition metal dichalcogenide nanosheets*, Nature Chem. **5**, 263 (2013); S. Z. Butler, S. M. Hollen, L. Y. Cao, Y. Cui, J. A. Gupta, H. R. Gutierrez, T. F. Heinz, S. S. Hong, J. X. Huang, A. F. Ismach, E. Johnston-Halperin, M. Kuno, V. V. Plashnitsa, R. D. Robinson, R. S. Ruoff, S. Salahuddin, J. Shan, L. Shi, M. G. Spencer, M. Terrones, W. Windl, J. E. Goldberger, *Progress, Challenges, and Opportunities in Two-Dimensional Materials Beyond Graphene*, ACS Nano **7**, 2898 (2013).
- [2] Q. H. Wang, K. Kalantar-Zadeh, A. Kis, J. N. Coleman, M. S. Strano, *Electronics and optoelectronics of two-dimensional transition metal dichalcogenides*, Nature Nanotech. **7**, 699 (2012).
- [3] C. Gaiser, T. Zandt, A. Krapf, R. Serverin, C. Janowitz, R. Manzke, *Band-gap engineering with  $HfS_xSe_{2-x}$* , Phys. Rev. B **69**, 075205 (2004).
- [4] C. Ruppert, O. B. Aslan, and T. F. Heinz, *Optical Properties and Band Gap of Single- and Few-Layer  $MoTe_2$  Crystals*, Nano Lett. **14**, 6231 (2014).
- [5] B. Sipos, A. F. Kusmartseva, A. Akrap, H. Berger, L. Forró and E. Tutiš, *From Mott state to superconductivity in  $1T-TaS_2$* , Nature Mater. **7**, 960 (2008).
- [6] D. E. Moncton, J. D. Axe, and F. J. Disalvo, *Neutron scattering study of the charge-density wave transitions in  $2H-TaSe_2$  and  $2H-NbSe_2$* , Phys. Rev. B **16**, 801 (1977); S. Bhattacharya, and M. J. Higgins, *Dynamics of a disordered flux line lattice*, Phys. Rev. Lett. **70**, 2617 (1993).
- [7] M. N. Ali, J. Xiong, S. Flynn, J. Tao, Q. D. Gibson, L. M. Schoop, T. Liang, N. Haldolaarachchige, M. Hirschberger, N. P. Ong and R. J. Cava, *Large, non-saturating magnetoresistance in  $WTe_2$* , Nature **514**, 205 (2014).
- [8] A. B. Pippard, *Magnetoresistance in Metals* (Cambridge University, Cambridge, 1989).
- [9] I. Pletikosić, M. N. Ali, A. V. Fedorov, R. J. Cava, and T. Valla, *Electronic Structure Basis for the Extraordinary Magnetoresistance in  $WTe_2$* , Phys. Rev. Lett. **113**, 216601 (2014).
- [10] J. Jiang, F. Tang, X. C. Pan, H. M. Liu, X. H. Niu, Y. X. Wang, D. F. Xu, H. F. Yang, B. P. Xie, F. Q. Song, X. G. Wan, and D. L. Feng, *Signature of strong spin-orbital coupling in the large non-saturating magnetoresistance material  $WTe_2$* , arXiv:1503.01422 (2015).
- [11] T. Liang, Q. Gibson, M. N. Ali, M. Liu, R. J. Cava, and N. P. Ong, *Ultrahigh mobility and giant magnetoresistance in the Dirac semimetal  $Cd_3As_2$* , Nature Mater. **14**, 280 (2015).
- [12] F.X. Xiang, M. Veldhorst, S.X. Dou, and X.L. Wang, *Multiple Fermi pockets revealed by Shubnikov-de Haas oscillations in  $WTe_2$* , arXiv:1504.01460 (2015).
- [13] Z. Zhu, X. Lin, J. Liu, B. Fauqué, Q. Tao, C. Yang, Y. Shi, and K. Behnia, *Quantum Oscillations, Thermoelectric Coefficients, and the Fermi Surface of Semimetallic  $WTe_2$* , Phys. Rev. Lett. **114**, 176601 (2015).
- [14] H. Y. Lv, W. J. Lu, D. F. Shao, Y. Liu, S. G. Tan, Y. P. Sun, *Perfect charge compensation in  $WTe_2$  for the extraordinary magnetoresistance: From bulk to monolayer*, arXiv:1412.8335 (2014).
- [15] B. Fauqué, H. Yang, I. Sheikin, L. Balicas, J.-P. Issi, and K. Behnia, *Hall plateaus at magic angles in bismuth beyond the quantum limit*, Phys. Rev. B **79**, 245124 (2009).
- [16] M. Shishkin, M. Marsman, and G. Kresse, *Accurate Quasiparticle Spectra from Self-Consistent GW Calculations with Vertex Corrections*, Phys. Rev. Lett. **99**, 246403 (2007).
- [17] F. Fuchs, J. Furthmüller, F. Bechstedt, M. Shishkin, and G. Kresse, *Quasiparticle band structure based on a generalized Kohn-Sham scheme*, Phys. Rev. B **76**, 115109 (2007).
- [18] M. Shishkin and G. Kresse, *Self-consistent GW calculations for semiconductors and insulators*, Phys. Rev. B **75**, 235102 (2007).
- [19] M. Shishkin and G. Kresse, *Implementation and performance of the frequency-dependent GW method within the PAW framework*, Phys. Rev. B **74**, 035101 (2006).
- [20] J. P. Perdew, K. Burke, and M. Ernzerhof, *Generalized Gradient Approximation Made Simple*, Phys. Rev. Lett. **77**, 3865 (1996).
- [21] P. E. Blöchl, *Projector augmented-wave method*, Phys. Rev. B **50**, 17953 (1994).
- [22] A. Kokalj, *Computer graphics and graphical user interfaces as tools in simulations of matter at the atomic scale*, Comp. Mater. Sci. **28**, 155 (2003), code available from <http://www.xcrysden.org/>.
- [23] Y. Zhao, H. Liu, J. Yan, W. An, J. Liu, X. Zhang, H. Jiang, Q. Li, Y. Wang, X.-Z. Li, D. Mandrus, X. C. Xie, M. Pan, J. Wang, *Anisotropic Magnetotransport and Exotic Longitudinal Linear Magnetoresistance in  $WTe_2$  Crystals*, arXiv:1502.04465 (2015).
- [24] See supplemental material at <http://link.aps.org>
- [25] P. Nozière and D. Pines, *Theory of quantum liquids*, ( W. A. Benjamin, New York, 1966).